Journal of Translational Medicine

RESEARCH

Open Access

Exploring the role of PARP1 inhibition in enhancing antibody–drug conjugate therapy for acute leukemias: insights from DNA damage response pathway interactions

Andrea Ghelli Luserna di Rorà[1,2], Mouna Jandoubi[1†], Antonella Padella[1,3†], Anna Ferrari[1*], Andrea Marranci[2], Cristina Mazzotti[1], Francesco Olimpico[2], Martina Ghetti[1], Lorenzo Ledda[1], Maria Teresa Bochicchio[1], Matteo Paganelli[1], Michele Zanoni[1], Alessandro Cafaro[4], Chiara Servili[1], Sara Galimberti[5], Michele Gottardi[6], Michela Rondoni[7], Mauro Endri[8], Daniela Onofrillo[9], Ernesta Audisio[10], Giovanni Marconi[1], Giorgia Simonetti[1] and Giovanni Martinelli[11]

Abstract

Background The introduction of antibody–drug conjugates represents a significant advancement in targeted therapy of acute myeloid leukemia (AML) and acute lymphoblastic leukemia (ALL). Our study aims to investigate the role of the DNA damage response pathway and the impact of PARP1 inhibition, utilizing talazoparib, on the response of AML and ALL cells to Gemtuzumab ozogamicin (GO) and Inotuzumab ozogamicin (INO), respectively.

Methods AML and ALL cells were treated with GO, INO and γ-calicheamicin in order to induce severe DNA damage and activate the G2/M cell-cycle checkpoint in a dose- and time-dependent manner. The efficacy of PARP1 inhibitors and, in particular, talazoparib in enhancing INO or GO against ALL or AML cells was assessed through measurements of cell viability, cell death, cell cycle progression, DNA damage repair, accumulation of mitotic DNA damage and inhibition of clonogenic capacity.

Results We observed that both ALL and AML cell lines activate the G2/M cell-cycle checkpoint in response to γ-calicheamicin-induced DNA damage, highlighting a shared cellular response mechanism. Talazoparib significantly enhanced the efficacy of INO against ALL cell lines, resulting in reduced cell viability, increased cell death, G2/M cell-cycle checkpoint override, accumulation of mitotic DNA damage and inhibition of clonogenic capacity. Strong synergism was observed in primary ALL cells treated with the combination. In contrast, AML cells exhibited a heterogeneous response to talazoparib in combination with GO. Our findings suggest a potential link between the differential responses of ALL and AML cells to the drug combinations and the ability of talazoparibto override G2/M cell-cycle arrest induced by antibody–drug conjugates.

†Mouna Jandoubi and Antonella Padella have contribututed equally to this work.

*Correspondence:
Anna Ferrari
anna.ferrari@irst.emr.it
Full list of author information is available at the end of the article

Conclusion PARP1 emerges as a key player in the response of ALL cells to INO and represents a promising target for therapeutic intervention in this leukemia setting. Our study sheds light on the intricate interplay between the DNA damage response pathway, PARP1 inhibition, and response of γ-calicheamicin-induced DNA damages in AML and ALL. These findings underscore the importance of targeted therapeutic strategies and pave the way for future research aimed at optimizing leukemia treatment approaches.

Keywords Antibody–drug conjugates, PARP1 inhibition, DNA damage response pathway, Acute myeloid leukemia (AML), Acute lymphoblastic leukemia (ALL)

Background

The introduction of antibody–drug conjugates (ADCs) represented a relevant advancement in terms of targeted therapy for acute leukemia patients [1–4]. ADCs combines monoclonal antibodies directed towards tumor-associated antigens with potent anti-neoplastic agents such as γ-calicheamicin [5]. Calicheamicin is a potent antitumor antibiotic that causes single strand breaks (SSBs) and double-strand DNA breaks (DSBs) and rapidly induces cell death by binding to the DNA's minor groove [6–8]. Nowadays, two ADCs, Gemtuzumab ozogamicin (GO) and Inotuzumab ozogamicin (INO), have been approved for the treatment of CD33-positive acute myeloid leukemia (AML) [9, 10] and CD22-positive acute lymphoblastic leukemia (ALL) [11] patients, respectively. In AML patients, GO was firstly approved as monotherapy for relapsed AML patients and then withdrawn because of a negative confirmatory trial and concerns for excess toxicity and death. It has been then re-approved for newly diagnosed adult and pediatric relapsed/refractory $CD33^+$ AML in combination with intensive chemotherapy. Regarding INO, following the success of as a salvage monotherapy, several trials are investigating its use as both salvage and frontline therapy in combination with low-intensity chemotherapy or other targeted anti-ALL therapies. In addition, INO is increasingly being used as a bridge therapy for allogeneic haematopoietic stem cell transplantation [12–14].

Preclinical and clinical studies have showed that several factors (expression level, polymorphism or mutations of the target, multi-drug resistance channels and others [15]) modify the efficacy of GO [4, 16–19] and INO [20–22] and are responsible for the development of treatment failure. For these reasons, the identification of novel drug combinations that can maximize the efficacy of ADCs in patients with acute leukemia remains an unmet clinical need.

In eukaryotic cells, a complex network known as DNA damage response (DDR) pathway, cooperates in the identification and repair of DNA damages [23]. Alterations in key DDR-related genes have been identified in several cancers and have been linked to genomic instability and chemo-resistance [24, 25]. In parallel, it has been shown that cancer cells depend on the functionality of DDR pathways in order to survive and continue to proliferate. The poly (ADP-ribose) polymerase 1 (PARP1) acts as a crucial DDR-mediator by adding PARylated chains to different DNA repair enzymes in the site of damage [24]. Indeed, PARP1 participates to various DNA repair pathways, including single strand break repair (SSBR) [26], homologous recombination (HR) [27], non-homologous end joining (NHEJ) [28] and base/nucleotide excision (NER/BER) [26] repair systems. Due to its central role in the response to DNA damages, PARP1 rapidly became an ideal target to enhance the efficacy of radio/chemotherapeutics [24, 29, 30]. Talazoparib, the last generation of PARP1/2 inhibitor, is currently proving its efficacy against acute leukemia at preclinical and clinical level in monotherapy or in combination with different compounds [24, 30–35].

This study evaluated whether the inhibition of PARP1 could enhance the effectiveness of GO and INO against AML and ALL cells and investigated the potential mechanism of action of the combinations.

Methods

Drugs and cell lines

The study used talazoparib, Gemtuzumab ozogamicin (GO), and Inotuzumab ozogamicin (IO) from Pfizer Oncology. Olaparib, veliparib and free calicheamicin were purchased from MedChemExpress (https://www.medchemexpress.com). Human ALL (KOPN-8, REH, SUP-B15 and RS4;11) and AML (KASUMI-1, KG-1, OCI-AML3, MOLM-13 and MV4-11) cell lines were cultured following manufacture's instruction (Deutsche Sammlung von Mikroorganismen and Zellkulturen GmbH,DSMZ, Braunschweig, Germany) and analyzed for CD22 (#130-128-400, Miltenyi Biotec, Bergisch Gladbach, Germany) and CD33 (#130-133-989, Miltenyi Biotec) expression. Flow cytometry analyses were performed using the Attune Nxt flow cytometer (ThermoFisher Scientific, Waltham, MA, USA) and mean fluorescence intensity was calculated using FlowJo v.10.8.1 software (BD Bioscience, Franklin Lakes, NJ, USA).

Primary samples

Human samples were obtained approval by Comitato Etico della Romagna (protocol n. 5244/2019, 5710/2020, 5805/2019) and collection of the informed consent. The study was carried out in accordance with the principles laid down in the 1964 Declaration of Helsinki. Mononuclear cells were obtained from peripheral blood or bone marrow samples of adult AML (n = 5) and ALL patients (n = 5) by using Histopaque-1077 solution (Merck-Millipore, Burlington, MA, USA). ALL cells were cultured in Advanced RPMI 1640 Medium (ThermoFisher Scientific) with 20% FBS, while AML cells were cultured in StemSpan™ SFEM-II Medium (STEMCELL Technologies, Vancouver, Canada) with 20 ng/mL, rh IL3, FLT3L, rhIL-6, rhSCF, rhG-CSF (PeproTech, London, UK), and 20% FBS.

Cell viability assay

AML and ALL cell lines were incubated with talazoparib (3000 to 12,3 nM, 1:3 dilution rate), olaparib (100 to 1,23 μM, 1:3 dilution rate), veliparib (100 to 1,23 μM, 1:3 dilution rate), GO (1473 to 2.02 ng/mL; 1:3 dilution rate), IO (1466 to 2.1 ng/mL; 1:3 dilution rate) and γ-calicheamicin (1 to 0.001 nM; 1:3 dilution rate) for 24, 48, and 72 h and cell viability was quantified using RealTime-Glo MT Cell Viability Assay (Promega, Madison, WI, USA) following manufacturer's instruction. Similarly, primary leukemic cells were treated with increasing concentrations of talazoparib (10.000 nM to 123 nM; 1:3 dilution rate), INO (1466 to 2.1 ng/mL; 1:3 dilution rate) or GO (1466 to 2.1 ng/mL; 1:3 dilution) for 24, 48 and 72 h. Viable cells were reported as a percentage of untreated controls (culture medium for GO and IO) or vehicle (DMSO for talazoparib). Inhibitory concentration 50 (IC_{50}) values were calculated using GraphPad Prism v.5 software (Dotmatics, Boston, MA, USA). The long-term effect of PARP1 inhibition has been evaluated after 5 days of treatments. Cell viability has been assessed using RealTime-Glo MT Cell Viability Assay (Promega) following manufacturer's instruction.

For combination index assay, AML and ALL cell lines were treated simultaneously with increasing concentrations of the test drugs (AML: Talazoparib + GO; ALL: Talazoparib + INO) for 24, 48, and 72 h (drugs' concentrations are reported in Table S1). The effect of the combination was quantified using Compusyn Software (Compusyn Inc.) and SynergyFinder online tool [36]. The first tool quantifies the additive, synergistic, and antagonistic effect of each drug-drug combinations and combination index (CI) is expressed as following: CI < 1 synergism, CI = 1 − 1.3 additivity, and CI > 1.3 antagonism. SynergyFinders quantifies the overall effect of the combinations using a Zero Interaction Potency (ZIP) model, which defines drugs interactions as either synergistic (synergy score > 10), additive (synergy score 10/− 10), or antagonistic (synergy score < − 10).

The effect of PARP1 inhibition in combination with calicheamicin-induced DNA damages was evaluated by treating AML and ALL cell lines with subtoxic concentrations of calicheamicin in combination with olaparib or veliparib for 24 and 48 h. The reduction of the cell viability was quantified by RealTime-Glo MT Cell Viability Assay (Promega) following manufacturer's instruction.

Apoptosis and cell-cycle analyses

For apoptosis and cell-cycle analyses, cells treated with talazoparib, GO or IO in single agent or in combination for 18, 24 (cell-cycle analysis) and 48 h (apoptosis and cell-cycles analysis; drug's concentrations are reported in Table S1). After treatment, cells were stained with eBioscience Annexin V Apoptosis Detection Kit (Invitrogen, Waltham, MA, USA) or propidium iodide staining mix (Sigma-Aldrich, St. Louis, MO, USA) and analysed by the Attune Nxt flow cytometer (ThermoFisher Scientific). The quantitative analyses were performed using Flowing software (Verity Software House).

Functional DNA damage response assay (UVC-ray response)

To investigate the overall DNA repair proficiency, we exposed AML and ALL cell lines to UV-ray as a non-chemical source of DNA damages [37]. Cells were exposed or not to UVC-ray (15 $J/m^2 \times 10''$) using BLX-e254 UV-Crosslinker (Vilber Lourmat, Eberhardzell, Germany) for 3 h and then $0.5X10^6$ cells were harvested and fixed with 95% ethanol/5% acetic acid followed by 1% formaldehyde, 0.25% Triton X-100 in TBS and stained with phospho-$H2AX^{Ser139}$-FITC conjugated antibody (Merck-Millipore) following manufacturer's instructions. The percentage of phospho-H2AX-positive cells was quantified using Attune Nxt Flow cytometer (ThermoFisher Scientific) The remaining cells were cultured for additional 21 h (total 24 h) and then counted by Trypan blue exclusion assay (Sigma Aldrich) to evaluate the cell viability.

Immunoblotting analysis

Immunoblotting analyses were performed using Mini-Protean TGX stain-free precast gels, blotted to nitrocellulose membranes (Bio-Rad, Hercules, CA, USA) and incubated the following antibodies: pATR ^{Ser428}(#2853); pATM^{Ser1981}(#5883); pCHK2^{Thr68}(#2661); pCHK1^{Ser345}(#2348); pWEE1^{Ser642}(#4910); ATM (#2873); ATR (#13934); CHK1 (#37010); CHK2 (#2662); WEE1 (#13,084); BRCA1 (#9010); BRCA2 (#10741); PALB2

(#30253); KU70 (#4588); XLF (#2854); PCNA (#13110); PARP1 (#9542); CCNB1 (#4138); pCDK1^{Tyr15} (#9111); pH2AX^{Ser139} (#2577); all from Cell Signaling Technologies (Danvers, MA, USA). The signal was detected using the enhanced chemiluminescence kit ECL (Bio-Rad, Hercules, CA, USA) and the compact darkroom ChemiDoc-It (Bio-Rad, Hercules, CA, USA). The intensity of the bands were analysed using ImageJ software (National Institutes of Health, Bethesda, MD, USA) as previously reported [38]. All the experiments have been performed in at least three independent experiments and immunoblotting analyses have been performed using independent cell lysates.

Phospho-H2AX and phospho-MPM2 staining

To evaluate the effect of the induction of DNA damages G2/M-arrested cells, ALL and AML cells were treated with sub-toxic concentrations of INO or GO for 48 h followed by talazoparib (IC_{50} values of each cell line) for additional 6 h. Then, cells were fixed and stained with anti-phospho-H2AX FITC conjugated antibody and with anti-phospho-Ser/Thr-Pro MPM-2 Antibody (Merck-Millipore) following manufacturer's instructions. All the flow cytometry analyses were performed using the AttuneNxt flow cytometer (ThermoFisher Scientific) and the quantitative analyses were performed using Flowjo software (BD Biosciences).

Comet assay

ALL and AML cells were treated with γ-calicheamicin (IC_{50} value) with or without talazoparib (IC_{50} value), harvested and seeded at 1×10^6/mL with 1% low melting point agarose in phosphate-buffered saline (PBS) at 37 °C to a final concentration of approximately 0.7%, and then transferred to comet slides. Slides were placed in pre-cooled lysis solution (2.5 M NaCl, 100 mM EDTA, 10 mM Tris, pH 10, 1% Triton X-100) for 1.5 h at 4 ℃. After lysis the slides were transferred to an electrophoresis slide tray containing pre chilled electrophoresis buffer (300 mM NaOH, 1 mM EDTA, pH > 13). Voltage was fixed at power source to 0.6 V/cm. After electrophoresis, slides were removed from chamber, drained, and submerged in neutralisation buffer (0.4 M Tris–HCl pH 7.5). Cells were then stained with Dapi solution and viewed on confocal microscope Olympus FV3000. Images were analysed using Fiji ImageJ software with Open Comet plugin. At least 50–100 randomly selected cells were analyzed per sample.

Clonogenic assay

Cells were seeded at $0.01X10^6$ cells/well in semi-solid medium added with 0.2% of Methyl-cellulose (Merck-Millipore) with or without subtoxic concentrations of calicheamicin (SUP-B15: 0.07 pM; REH: 2 pM; RS4;11: 0.0013 pM; KOPN-8: 0.2 pM; OCI-AML3: 5 pM; KG-1: 7.5 pM; MV4-11: 2 pM; MOLM-13: 0.3 pM; KASUMI-1:0.02 pM) in combination with talazoparib (SUP-B15: 0.00019 μM; REH: 0.055 μM; RS4;11: 0.0016 μM; KOPN-8: 0.0055 μM; OCI-AML3: 0.166 μM; KG-1: 0.05 μM; MV4-11: 0.33 μM; MOLM-13: 0.06 μM; KASUMI-1:0.11 μM). After 10–14 days, the experiments were stopped and the colonies were photographed (Nikon Eclipse Ci microscope). The number of the colonies were automatically analysed using ImageJ software.

Statistical analyses

Data are presented as mean ± standard deviation of at least three independent experiments or biological replicates. Pearson correlation analysis, two-tailed t tests or two-way ANOVA tests were used to assess statistical significance by Graphpad v.5 software (GraphPad Inc., San Diego, CA, USA). Statistical significance is expressed as p value (*$p \le 0.05$; **$p \le 0.01$; ***$p \le 0.001$). The data supporting the conclusions are included within the article and its Supplementary Material.

Results

ALL and AML cell lines respond to calicheamicin-induced DNA damages by activating the G2/M cell-cycle checkpoint

We firstly evaluated the efficacy of GO and INO against a panel of AML (KASUMI-1, KG-1, OCI-AML3, MOLM-13 and MV4-11) and ALL (KOPN8, REH, SUP-B15 and RS4;11) cell lines. The different cell lines have been chosen based on their molecular and cytogenetic background as they represent diverse acute leukemia subtypes. A significant heterogeneity in terms of reduction of the cell viability in response to ADCs was observed among them. KASUMI-1 (IC_{50} at 24 h: 1.14 ng/mL) and SUP-B15 (IC_{50} at 24 h: 9.45 ng/mL) were the most sensitive cell lines to GO and INO, respectively, while OCI-AML3 (IC_{50} at 24 h: 18.7 μg/mL) and REH (IC_{50} at 24 h: 319.7 ng/mL) showed the lowest response (Fig. 1A; Table 1). We asked whether such heterogeneity in terms of response was associated with the levels of expression of CD22 (INO) or CD33(GO). In line with observations from the several clinical trials [39, 40], we found that the expression of CD33 positively correlates with response to GO after 48 and 72 h of treatment (Fig. 1B). Conversely, in ALL cell lines no significant correlation was found.

To discriminate the potential cofounding effect of target expression in the evaluation of ADC response, we treated the cells with γ-calicheamicin alone. We confirmed that the AML and ALL cell lines exhibiting the highest response to the corresponding ADCs were also the most sensitive to γ-calicheamicin (Fig. 1C, Table 1).

We thus sought to address whether the heterogenous sensitivity of acute leukemia cell lines to ADCs was linked to their capability to respond to γ-calicheamicin-induced DNA damage. We firstly evaluated the effect of INO and GO on the activation of cell-cycle checkpoints as a consequence of DNA damage induction. Both ADCs significantly modified the cell-cycle profile of AML and ALL cell lines by inducing a significant G2/M-phase arrest, while reducing the number of cells in the G1 and S phase (Fig. 1D). The induction of the G2/M cell cycle arrest was then confirmed by immunoblotting analysis (Fig. 1E, F, S1A-S1B). In ALL, we observed a significant induction of phospho-CDK1^{Tyr15} and Cyclin B1 expression, which represent the mitotic promoting factors (MPF complex) regulating the transition from G2 to M phase. As expected, INO induced DNA damages in ALL cell lines, as shown by the induction of phospho-H2AX-^{Ser139} (Fig. 1E, 1G). Focusing on GO, we found a significant increase of CCNB1 in OCI-AML3 and KG-1 cells and an increase of phospho-CDK1^{Tyr15} in all the cell lines with the exception of MOLM-13 cells. Finally, GO significantly induced DNA damages (phospho-H2AX^{Ser139}) in all the treated AML cell lines with the exception of MV4-11, in which only a trend of increase could be detected (Fig. 1F, G). To deeper investigate the involvement of the G2/M cell cycle checkpoint in the response to ADCs we performed immunoblotting analyses focusing on the activation of cell cycle checkpoint kinases. Sub-toxic concentrations of γ-calicheamicin led to activation of both the ATR/CHK1 and the ATM/CHK2 pathways in ALL cell lines. In AML cells, only MV4-11 and KG-1 cells exhibited a similar response (Fig. 1H, I, S1C). Despite significant heterogeneity, we found that the activation of the G2/M checkpoint was confirmed by a reduction in phospho-WEE1^{ser642} levels in nearly all tested cell lines, including RS4;11, KOPN-8, SUP-B15, KASUMI-1, and MOLM-13..

ALL cell lines are more sensitive to PARP inhibitors and to single strand breaks inducers compared to AML cells

Before assessing whether PARP1 inhibition could improve ADC's cytotoxicity, we evaluated the impact of single agents veliparib, olaparib and talazoparib in ALL and AML cell lines. The three compounds share the ability to inhibit PARP1 functionality with different specificity and are differentially able to induce PARP1 trapping on DNA [41]. Talazoparib was the most effective agent, inducing a dose- and time-dependent decrease in cell viability in all treated cells, with ALL cells showing greater sensitivity than AML cell lines, although this was not statistically significant (Fig. 2A; Table 2). In particular, SUP-B15 demonstrated the highest sensitivity (IC_{50} at 24 h: 24 nM), while MV4-11 exhibited the lowest sensitivity (IC_{50} at 72 h: 52 μM) to talazoparib.. Consistently, SUP-B15 and MV4-11 were respectively the most and least sensitive cells to olaparib and veliparib (Table 2). Similar results have been obtained by evaluating the long-term exposure to PARP1 inhibitors against ALL and AML cells. Indeed, ALL showed a greater sensitivity compared to AML cells to PARP1 inhibitors after 5 days of treatment (Fig.S2A).Based on the enhanced efficacy of talazoparib in the reduction of cell viability, we decided to better investigate its mechanism of action and to correlate its response to the molecular background and DNA repair proficiency of AML and ALL cell lines. Preliminarily, we consulted genomic online databases (Cosmic, Cell model passport and Cacner Cell Line Encyclopedia [42, 43]) searching for inactivating mutations or other genetic alterations in DDR genes known to modify the response

(See figure on next page.)

Fig. 1 Effect of INO, GO and γ-calicheamicin on cell viability, cell-cycle perturbation and G2/M checkpoint activation in ALL and AML cell lines. **A** Reduction of the cell viability of ALL (blue) and AML (red) cell lines treated for 24, 48 and 72 h with increasing concentration of INO and GO, respectively. Each point represents the mean ± standard deviation of normalized cell viability obtained from at least three independent experiments. Dashed lines represent the indicative values of inhibitory concentration 50 (IC_{50}). **B** Expression of CD33 and CD22 in AML (red) and ALL (blue) cell lines by flow cytometry. Histograms represent the mean and standard deviation of the mean fluorescence intensity (MFI) of AML and ALL cell lines obtained from at least three independent experiments. The table reports the Pearson correlation coefficient in AML and ALL cell lines between CD22 expression and IC_{50} values after 24, 48 and 72 h of GO and INO, respectively. **C** Reduction of the cell viability of ALL (blue) and AML (red) cell lines treated for 24, 48 and 72 h with increasing concentrations of γ-calicheamicin. Each point represents the mean ± standard deviation of normalized cell viability obtained from at least three independent experiments. Dashed lines represent the indicative values of inhibitory concentration 50 (IC_{50}). **D** Cell-cycle profile analysis of ALL and AML cell lines treated for 18, 24 and 48 h with subtoxic concentrations of INO (near IC_{50} values after 24 h) and GO (near IC_{50} values after 24 h), respectively. **E**, **F** Representative immunoblotting analysis of ALL and AML cell lines treated with INO (near IC_{50} values after 24 h) or GO (near IC_{50} values after 24 h) for 18 h. β-actin was used for loading normalization. **G** Histograms representing the mean ± standard deviation the relative bands intensity of CCNB1, phospho-CDK1^{Tyr15} and phospho-H2AX^{Ser139} proteins in ALL (blue) and AML (red) cell lines treated INO or GO for 18 h. **H** Immunoblotting analysis of ALL and AML cell lines treated with γ-calicheamicin (IC_{50} values after 24 h) for 18 h. β-actin was used for loading normalization. **I** Histograms represent the mean and standard deviation the relative bands intensity of phospho-ATM^{Ser1981}, phospho-ATR^{Ser428}, phospho-CHK2^{Thr68}, phospho-CHK1^{Ser345} and phospho-WEE1^{Ser642} proteins in ALL (blue) and AML (red) cell lines treated INO or GO for 18 h. All error bars represent the mean ± SD

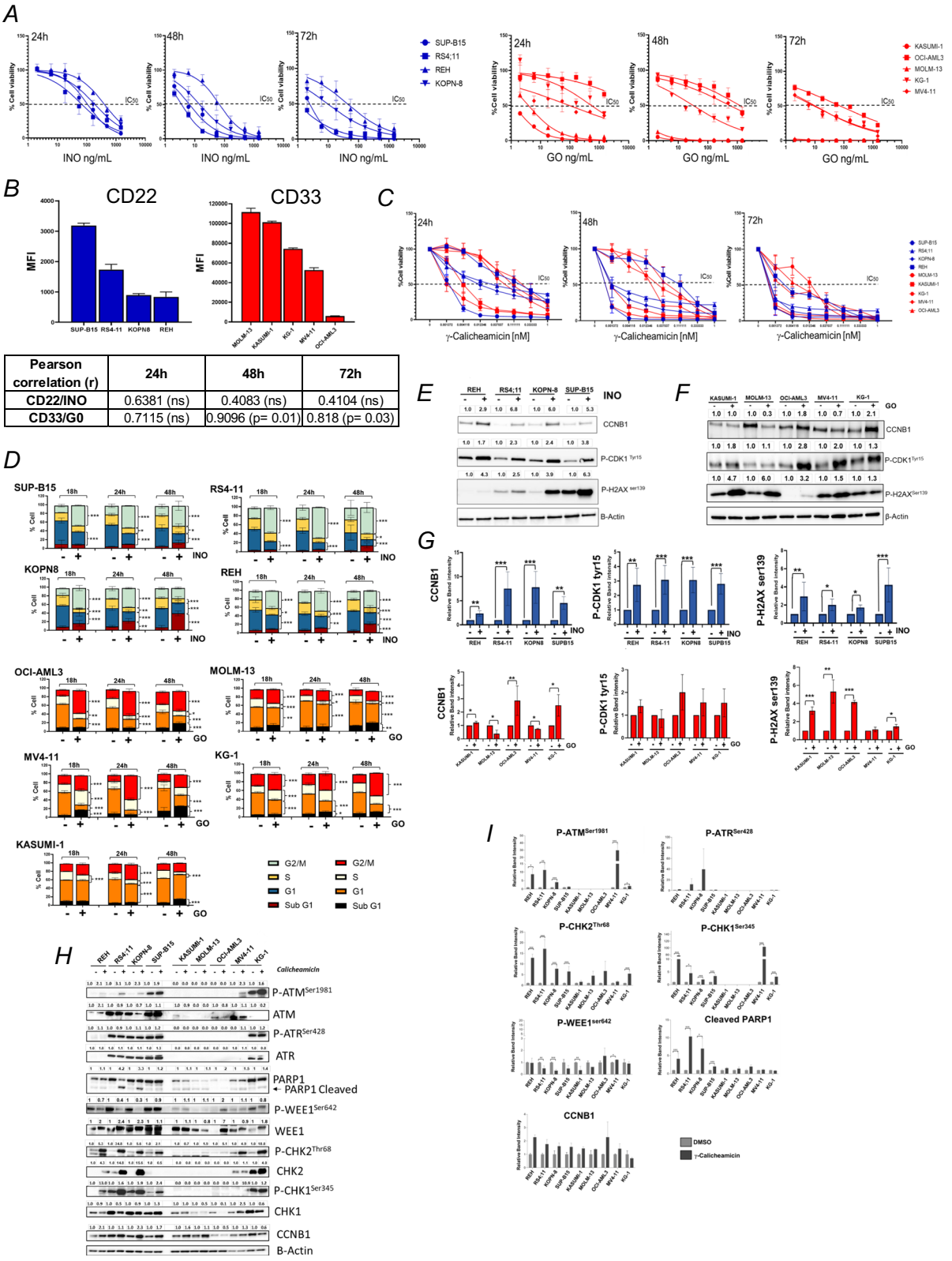

Pearson correlation (r)	24h	48h	72h
CD22/INO	0.6381 (ns)	0.4083 (ns)	0.4104 (ns)
CD33/G0	0.7115 (ns)	0.9096 (p= 0.01)	0.818 (p= 0.03)

Fig. 1 (See legend on previous page.)

Table 1 IC_{50} values of AML and ALL cell lines treated with GO, INO or γ-calicheamicin as single agents

IC_{50}	24 h	48 h	72 h
Gemtuzumab ozogamicin (GO, ng/mL)			
KASUMI-1	1.14	0.15	0.27
OCI-AML3	18,787	1120	66.7
MOLM-13	3.58	0.23	0.017
KG-1	501.6	29.13	9.30
MV4-11	477.1	510	8.38
Inotuzumab ozogamicin (INO, ng/mL)			
SUP-B15	9.45	0.58	0.22
REH	319.7	55.16	34.73
RS4;11	53.8	2.88	0.75
KOPN8	149.1	11.73	7.72
γ-calicheamicin (pM)			
KASUMI-1	1.011	0.08079	0.01589
OCI-AML3	130.5	32.43	6.94
MOLM-13	4.678	0.8594	0.193
KG-1	77.79	19.27	10.49
MV4-11	174.3	57.83	2.441
SUP-B15	1.574	0.5606	0.007481
REH	157.6	81.16	3.095
RS4;11	29.27	0.6273	0.001039
KOPN8	20.04	0.5876	0.1517

to PARP1 inhibitors. No alterations affecting the sensitivity to PARP1 inhibition was identified. Therefore, we evaluated the level of expression and the functionality of the DDR machinery. Firstly, we analyzed the expression of key proteins involved in HR (BRCA1, BRCA2 and PALB2), NHEJ (KU70, XLF and DNA-PK) and SSBR (PARP1 and PCNA) repair systems (Fig. 2B, S2B). We did not observe any correlation between the response to talazoparib (IC_{50} values) and the basal level of expression of these proteins in the analyzed cell lines. However, considering the two groups of leukemias, we found that ALL models, that display a higher sensitivity to talazoparib, expressed significantly higher levels of BRCA1, BRCA2, PCNA and PARP1 proteins compared with AML ones (Fig. 2C, S2C). Subsequently, we investigated the DNA repair proficiency of AML and ALL cell lines by evaluating their response to UV rays, as a non-chemical source of DNA damage. Flow cytometry analysis of phospho-H2AX^{Ser139} showed a significantly different response to UV-damages expressed as DBS induction. In particular, after UV exposure, AML cell lines expressed lower level of phospho-H2AX^{Ser139} compared with ALL cells (Fig. 2D). In details, we observed a significant increase of phospho-H2AX^{Ser139} expression in REH, RS4;11 and KOPN8 cells. In terms of cytotoxicity, ALL cells were more sensitive to UV ray exposure compared with AML ones, with a 50% decrease of cell viability of UV-treated cells compared to untreated cells (Fig. 2E). Finally, we evaluated the effect of talazoparib on the cell-cycle profile. AML and ALL cell lines showed a heterogeneous response. Indeed, depending on the cell line and the drug exposure, talazoparib increased or reduced the percentage of cells in S and G2/M phase (Fig. 2F).

Talazoparib enhances the efficacy of INO by interfering with the G2/M cell-cycle checkpoint stability in ALL cell lines.

To evaluate whether the inhibition of PARP1 potentiate the anti-leukemic effect of ADCs, we performed combination index (CI) analyses using sub-toxic concentrations of INO and talazoparib. We observed a significant reduction of the cell viability in all ALL cell lines treated with the combination (Fig. 3A). CI analyses and ZIP score analysis highlighted that the efficacy of the combination shifted from antagonism to strong synergism depending on drug concentrations and time of exposure, with the highest efficacy being observed at

(See figure on next page.)

Fig. 2 Effect of PARP1 inhibition on cell viability, cell-cycle regulation and DDR in ALL and AML cell lines. **A** Reduction of the cell viability of ALL (blue) and AML (red) cell lines treated for 24, 48 and 72 h with increasing concentration of veliparib, olaparib or talazoparib. Each point represents the mean ± standard deviation of normalized cell viability obtained from at least three independent experiments. Dashed lines represent the indicative values of inhibitory concentration 50 (IC_{50}). **B** Representative immunoblot showing the basal expression level of proteins from different DDR pathways. β-actin was used for loading normalization. **C** Box-plots showing the distribution of the normalized protein levels (normalization: bands intensity of protein of interest/band intensity of β-actin) in ALL (n = 5; blue) and AML (n = 5; red) cell lines. In the graph, the box-plots represent the distribution of the mean values of at least two independent experiments. **D** Histograms show the percentages of phospho-H2AX^{Ser139} expressing cells after 3 h from the exposure to UVC ray in ALL (blue) and AML (red) cells. The left panel of the figure represents the effect of all cell lines together while the right panel represents the effect of each cell lines. In the graph, histograms represent the results of at least three independent experiments. **E** Cell viability of AML and ALL cell lines after 24 h from UV-ray exposure. The left panel of the figure represents the normalized cell viability (UV-treated/untreated cells) of all cell lines together while the right panel represents the effect of each cell line. Histograms represent the results of at least three independent experiments. **F** Effect of subtoxic concentrations of talazoparib on cell-cycle profiles of ALL (RS4;11 = 333.3 nM, REH = 1000 nM, KOPN8 = 111.1 nM and SUP-B15 = 37.0 nM) and AML (KASUMI-1 = 3000 nM, MOLM-13 = 3000 nM, OCI-AML3 = 3000 nM, MV4-11 = 1000 nM and KG-1 = 1000 nM) cell lines treated for 18, 24 and 48 h. The different cell-cycle-phases are represented as percentage of cells. All error bars represent the mean ± SD

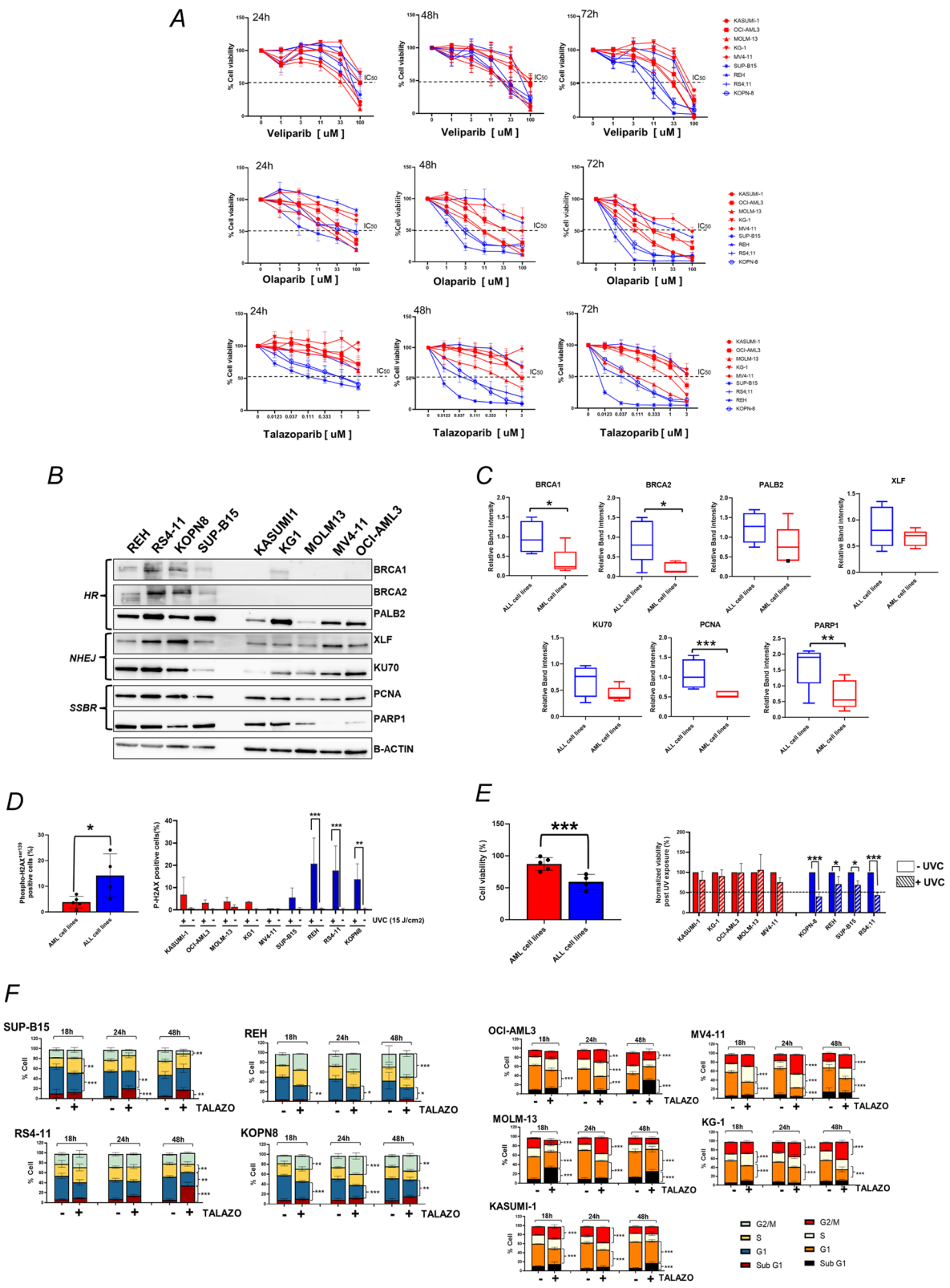

Fig. 2 (See legend on previous page.)

Table 2 IC_{50} values of AML and ALL cell lines treated with talazoparib, olaparib or veliparib as single agent

PARP inhibitor	**Talazoparib [μM]**	**Olaparib [μM]**	**Veliparib [μM]**
IC_{50}	**24 h**		
KASUMI-1	19.83	32.2	42.05
OCI-AML3	8.57	55	101.9
MOLM-13	8.32	18.58	27.23
KG-1	3.55	177	105.8
MV4-11	52.95	776.3	59.64
SUP-B15	0.24	9.252	58.02
REH	9.69	238.1	90.32
RS4;11	1.07	66.08	124
KOPN8	1.02	54.73	98.86
IC_{50}	**48 h**		
	Talazoparib [μM]	**Olaparib [μM]**	**Veliparib [μM]**
KASUMI-1	8.15	11.08	19.62
OCI-AML3	3.15	33.71	81.22
MOLM-13	0.73	8.343	14.3
KG-1	3.3	54.29	105
MV4-11	7.55	376.1	83.09
SUP-B15	0.04	1.288	20.16
REH	7.8	149.8	64.59
RS4;11	0.41	3.677	18.72
KOPN8	0.9	4.501	31.45
IC_{50}	**72 h**		
	Talazoparib [μM]	**Olaparib [μM]**	**Veliparib [μM]**
KASUMI-1	4.24	4.901	29.69
OCI-AML3	1.74	15.88	46.79
MOLM-13	0.92	3.61	27.22
KG-1	0.68	19.58	88.39
MV4-11	5.9	116.2	70.18
SUP-B15	0.02	0.8496	6.529
REH	2.57	40.9	59.1
RS4;11	0.34	1.321	12.77
KOPN8	0.73	1.692	13.75

72 h (Fig. S3A). The SUP-B15 cells were identified as the most sensitive cells ($\delta = 18.27$, strong synergism), while the KOPN-8 cells were determined to be the least sensitive ($\delta = 4.98$, additive; Fig. 3B; Table S1). To confirm the role of PARP1 inhibition in enhancing the cytotoxicity of γ-calicheamicin, we treated ALL cell lines with subtoxic concentrations of γ-calicheamicin with and without talazoparib, veliparib, or olaparib. Consistent with previous results, the inhibition of PARP1 by talazoparib significantly increased the cytotoxicity of γ-calicheamicin in ALL cell lines, with SUP-B15 proving to be the most sensitive model to this combination. Olaparib and veliparib also enhanced the cytotoxic effects of γ-calicheamicin, although this enhancement varied among the different cell lines, with SUP-B15 again showing the highest sensitivity. Additionally, we observed that REH cells were significantly more sensitive to the combination of veliparib and γ-calicheamicin compared to the single treatments and control conditions. (Fig. 3C). We then addressed whether the inhibition of cell viability was associated with an increased cell death and we observed that INO combined with talazoparib significantly enhanced apoptosis in ALL cell lines compared with single agent treatments and controls (Fig. 3D). To deeply investigate the mechanism of action of this combination, we performed cell-cycle

analysis in ALL cell lines treated with INO and talazoparib for 18, 24 and 48 h. In the samples treated with the combinations, we observed a progressive reduction of the percentage of cells in G2/M phase compared with INO in single agent, that was in line with the effect of talazoparib as single agent (Fig. 3E, F, Table S2). Immunoblotting analysis performed on ALL cell lines confirmed the effect of the combination on the G2/M cell-cycle checkpoint stability and in the induction of DNA damages and cell death. We observed a significant increase of phospho-H2AX^{Ser139} and cleaved CASP3 in SUP-B15, REH and KOPN-8 cells. IN RS4;11 cells we found a significant increase of phospho-H2AX^{Ser139} and a trend of increase of cleaved CASP3, although not significant. Regarding the effect of combination on the G2/M cell-cycle checkpoint, in all the treated ALL cells we found a trend of reduction of the MPF complex (CCNB1 or phospho-CDK1^{Tyr15}) levels in the samples treated with the combination in comparison with INO alone (Fig. 3G, S3B). We then assessed the potential fate of the G2/M arrested cells (as induced by INO treatment) when forced by talazoparib to progress to cell division by evaluating the induction of DNA damages in mitotic cells. Therefore, we treated ALL cell lines with INO for 48 h followed by talazoparib for additional 6 h and stained cells with anti phospho-H2AX-^{Ser139} antibody and anti-phospho-Ser/Thr-Pro MPM-2 antibody, as a marker of mitotic activity [44]. Compared with the control cells treated with DMSO, the percentage of pH2AX^{+}/pMPM2^{+} cells progressively increased in the samples treated with talazoparib or INO or with their sequential combination (Fig. 3H). The most significant effect of the combinations in comparison with control and single treatments was observed in KOPN8 cells. We then evaluated the effect of talazoparib in the repair of γ-calicheamicin-induced DNA damages using Comet assay in SUP-B15 cells. We found a significant increase of DNA damages in the combination compared to control and single treatments expressed as comet' tail moment, area and length suggesting an active role of PARP1 in the repair of calicheamicin-induced DNA breaks (Fig. 3I). Lastly, we evaluated the effect of long-term exposure to talazoparib and INO or γ-calicheamicin in term of inhibition of clonogenic capacity. In all the treated cells the exposure to talazoparib in combination with INO or γ-calicheamicin significantly reduced the clonogenic capacity compared to controls and single treatments (Fig. 3J, K).

(See figure on next page.)

Fig. 3 Talazoparib enhances INO and γ-calicheamicin cytotoxicity in ALL cell lines in terms of reduction of cell viability, induction of apoptosis and DNA damage. **A** Heatmaps showing the effect on cell viability of subtoxic concentrations of INO in combination with talazoparib for 72 h in ALL cells. In the heatmaps, the color scale represents the values of mean normalized cell viability (% of cell viability relative to control) of at least three independent experiments. The white number inside each square of the heatmap represents the combination index (CI) value. C.I < 1 means synergism; C.I = 1–1.3 means additivity; C.I > 1.3 means antagonist; **B** two-dimensional ZIP synergy map of ALL cell lines treated with increasing concentrations of INO and talazoparib for 72 h. Zero Interaction potency (ZIP) score is expressed as δ value. The black cross represents the highest values of ZIP score for each combination. **C** Reduction of cell viability of ALL cell lines treated with γ-calicheamicin (RS4;11 = 25 pM; REH = 160 pM; SUP-B15 = 3 pM; KOPN-8 = 20 pM) in combination with talazoparib (RS4;11 = 1 μM; REH = 5 μM; SUP-B15 = 0.2 μM; KOPN-8 = 1 μM), olaparib (RS4;11 = 10 μM; REH = 50 μM; SUP-B15 = 3 μM; KOPN-8 = 54 μM) or veliparib (RS4;11 = 70 μM; REH = 100 μM; SUP-B15 = 50 μM; KOPN-8 = 98 μM) for 24 h. Histograms represent the mean and standard deviation of normalized cell viability of three independent experiments. **D** Histograms represent the percentage of Annexin V + cells of CD22-positive ALL cell lines treated with INO (SUP-B15 = 4.9 ng/mL, RS4;11 = 14.7 ng/mL, KOPN-8 = 44.2 ng/mL and REH = 14.7 ng/mL) and talazoparib (SUP-B15 = 37.0 nM, RS4;11 = 333.3 nM, KOPN8 = 111.1 nM and REH = 1000 nM) for 48 h (results of at least three independent experiments). **E** Histograms represent the percentage of cells in different cell-cycle phases after 18, 24 and 48 h of treatment with INO alone or in combination with talazoparib. ALL cell lines were treated with INO (SUP-B15 = 4.9 ng/mL, RS4;11 = 14.7 ng/mL, KOPN-8 = 44.2 ng/mL and REH = 14.7 ng/mL) and/or talazoparib (SUP-B15 = 37.0 nM, RS4;11 = 333.3 nM, KOPN8 = 111.1 nM and REH = 1000 nM). Histograms represent mean ± standard deviation of at least three independent experiments. **F** Histograms represent the variation of G2/M and S phase cells between INO in combination with talazoparib and cells treated with INO alone. Positive fold-change (FC) indicates increased values while negative FC indicates decreased values. **G** Immunoblot analysis of ALL cells treated with INO (SUP-B15 = 4.9 ng/mL; RS4;11 = 14.7 ng/mL; KOPN8 = 44.27 ng/mL; REH = 14.7 ng/mL,) and talazoparib (SUP-B15 = 37.0 nM; RS4;11 = 333.3 nM; KOPN8 = 111.1 nM; REH = 1000 nM) for 24 h. β-actin was used for loading normalization. The numbers above the bands represent the relative quantification of band intensity. On the right, histograms represent the average signal obtained from relative band quantification of at least three independent experiments. **H** Histograms showing the percentage of pH2AX^{+}/pMPM2^{+} cells in ALL cell lines treated with subtoxic concentrations of INO for 48 h and with talazoparib (IC_{50} values after 24 h of treatment) for additional 6 h. **I** Comet assay in SUP-B15 cell lines treated with γ-calicheamicin (IC_{50} value) in combination with talazoparib (IC_{50} value) for 18 h. Scatter-plots with histograms show the variation of Tail Area, Tail Length and Tail moment between controls and treatments. **J** Clonogenic results of RS4;11, REH, SUP-B15 and KOPN-8 cells treated with sub-toxic concentrations of γ-calicheamicin (SUP-B15 = 0.07 pM; REH = 2 pM; RS4;11 = 0.0013 pM; KOPN-8 = 0.2 pM) and talazoparib (SUP-B15 = 0.00019 μM; REH = 0.055 μM; RS4;11 = 0.0016 μM; KOPN-8 = 0.0055 μM) for 10–14 days. **K** Clonogenic results of RS4;11, REH, SUP-B15 and KOPN-8 cells treated with sub-toxic concentrations of INO (SUP-B15 = 4.8 ng/mL; RS4;11 = 17.4 ng/mL ng/mL; KOPN8 = 48 ng/mL; REH = 4.8 ng/mL) and talazoparib (SUP-B15 = 0.00019 μM; REH = 0.055 μM; RS4;11 = 0.0016 μM; KOPN-8 = 0.0055 μM) for 10–14 days

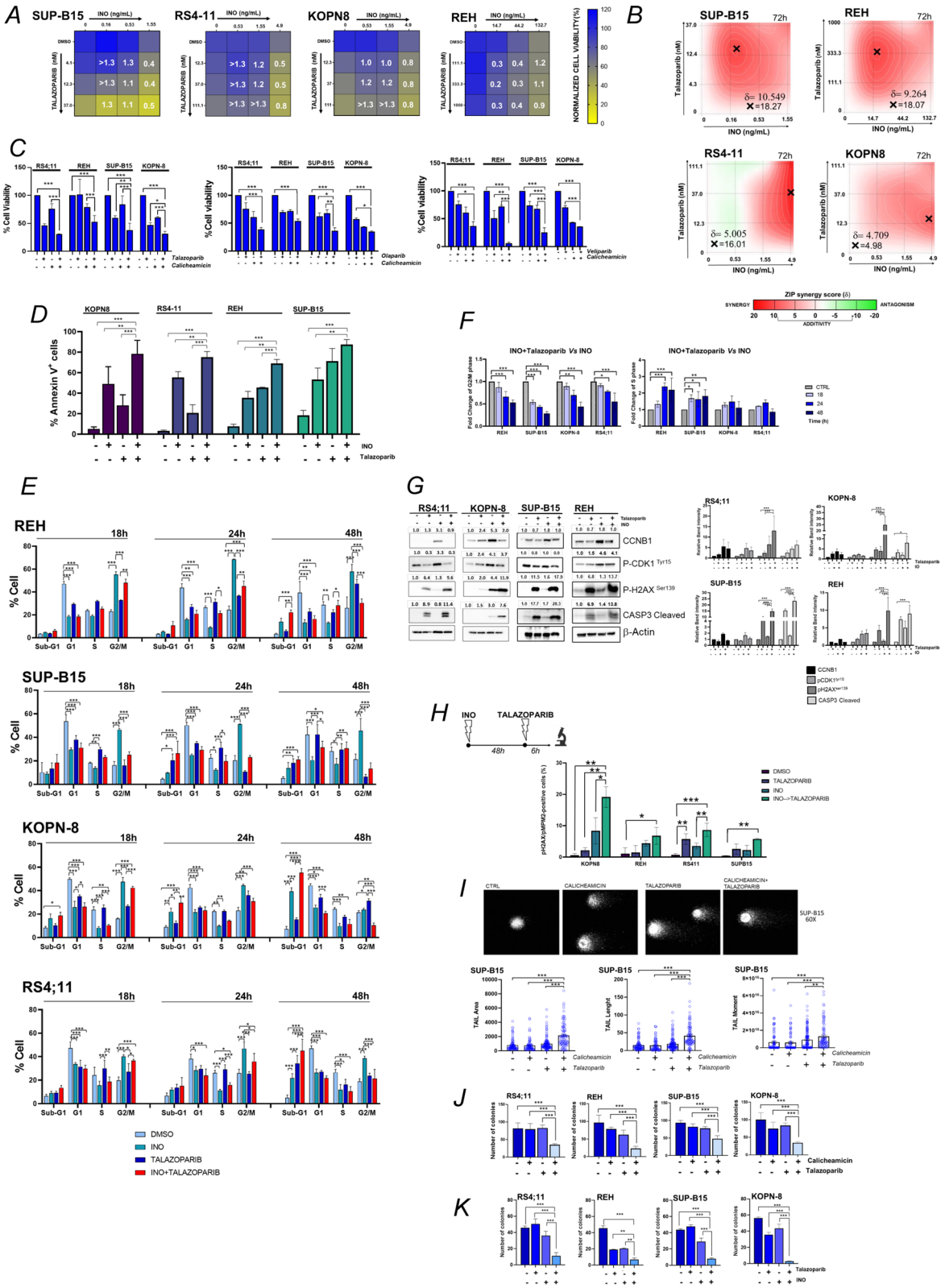

Fig. 3 (See legend on previous page.)

AML cell lines display a heterogeneous response of talazoparib in combination with GO

The efficacy of combining GO with PARP1 inhibitors has been suggested by previous studies on HL-60 and HEL cellular models [45, 46]. We here evaluated the efficacy of combining GO and talazoparib in our panel of AML cell lines. The combination index analyses and ZIP synergy score showed that the efficacy of the combination was dependent on the leukemia model, the dose and the time of exposure with KG-1, OCI-AML3 and MV4-11 being the most sensitive while KASUMI-1 and MOLM-13 the lowest sensitive cells (Fig. 4A, B; S4A; Table S3). As for ALL cell lines, we evaluated the efficacy of combining γ-calicheamicin with different PARP1 inhibitors. The results of the experiments confirmed that OCI-AML3 cells were the most sensitive models while MOLM-13 and KASUMI-1 the least sensitive (Fig. 4C). In terms of induction of cell death, OCI-AML3 and MOLM-13 confirmed to be the most and least sensitive cells to the combination, respectively (Fig. 4D). The combination of GO and talazoparib heterogeneously altered the cell-cycle profile of treated cells, with only OCI-AML3 cells showing a significant and progressive reduction in G2/M arrest induced by GO (Fig. 4E, F). Immunoblotting confirmed this effect, showing reduced levels of phospho-CDK1^{Tyr15} after 24 h of co-treatment. Additionally, the combination treatment led to enhanced DNA damage in OCI-AML3 cells compared to the control and talazoparib alone, and in MV4-11 cells compared to the control and GO alone. In KG-1 cells, we observed a progressive induction of pH2AX (Ser139) and cleaved CASP-3 with the combination treatment, compared to both the control and single treatments. In MOLM-13 and KASUMI-1 cells, the combination did not alter the levels of phospho-CDK1^{Tyr15} or CCNB1; however, we reported an increased induction of DNA damage compared to controls and GO as a single agent, but not when combined with talazoparib. (Fig. 4G, S4B). The quantification of pH2AX$^+$/pMPM2$^+$ cells did not show a significant increase in double positive cells between samples treated with GO in combination with talazoparib compared to single treatments (Fig. 4H). To investigate whether the treatment with talazoparib inhibits the overall capacity of repairing γ-calicheamicin-induced DNA damages, we performed Comet assay on OCI-AML3 cells, which were sensitive to the combination. The combination significantly enhanced DNA damages as showed by comet tail moment, area and length (Fig. 4I). Finally, we evaluated

(See figure on next page.)

Fig. 4 Effect of talazoparib in combination with GO against AML cell lines. **A** Heatmaps showing the effect on cell viability of subtoxic concentrations of GO in combination with talazoparib for 72 h in AML cells. In the heatmaps, the color scale represents the values of mean normalized cell viability (% of cell viability relative to control) of at least three independent experiments. The white number inside each square of the heatmaps represents the combination index (C.I) values. C.I < 1 means synergism; C.I = 1–1.3 means additivity; C.I > 1.3 means antagonist; NC = combination index Not Calculable using Compusyn software. **B** Two-dimensional synergy map of AML cell lines treated with increasing concentrations of GO and talazoparib for 72 h. Zero Interaction Potency (ZIP) score is expressed as δ value. **C** Reduction of cell viability of AML cell lines treated with γ-calicheamicin (OCI-AML3 = 150 pM; KG-1 = 70 pM; MV4-11 = 150 pM; MOLM-13 = 4.7 pM; KASUMI-1 = 1.9 pM) in combination with olaparib (OCI-AML3 = 50 μM; KG-1 = 100 μM; MV4-11 = 200 μM; MOLM-13 = 18 μM; KASUMI-1 = 32 μM) or veliparib (OCI-AML3 = 100 μM; KG-1 = 100 μM; MV4-11 = 100 μM; MOLM-13 = 27 μM; KASUMI-1 = 42 μM) for 24 h. Histograms represent the mean ± standard deviation of normalized cell viability of three independent experiments. **D** Histograms represent the percentage of Annexin V + cells of AML cell lines treated with GO (OCI-AML3 = 1473 ng/mL; KG-1 = 1473 ng/mL; MV4-11 = 1473 ng/mL; MOLM-13 = 1.97 ng/mL; KASUMI-1 = 1.97 ng/mL) and talazoparib (OCI-AML3 = 3 μM; KG-1 = 3 μM; MV4-11 = 3 μM; MOLM-13 = 3 μM; KASUMI-1 = 3 μM) for 48 h (results of at least three independent experiments). **E** Histograms represent the percentage of cells in different cell-cycle phases after 18, 24 and 48 h of treatment with GO (OCI-AML3 = 1473 ng/mL; KG-1 = 1473 ng/mL; MV4-11 = 1473 ng/mL; MOLM-13 = 1.97 ng/mL; KASUMI-1 = 1.97 ng/mL) and/or talazoparib (OCI-AML3 = 3 μM; KG-1 = 3 μM; MV4-11 = 3 μM; MOLM-13 = 3 μM; KASUMI-1 = 3 μM). Histograms represent mean and standard deviation of at least three independent experiments. **F** Histograms represent the variation of G2/M and S phase cells between GO in combination with talazoparib and cells treated with GO alone. Positive fold-change (FC) indicates increased values while negative FC indicates decreased values. Asterisks indicate statistical significance of each condition compared to control cells. **G** Immunoblot analysis of AML cells treated with GO (OCI-AML3 = 1473 ng/mL; KG-1 = 1473 ng/mL; MV4-11 = 1473 ng/mL; MOLM-13 = 1.97 ng/mL; KASUMI-1 = 1.97 ng/mL) and talazoparib (OCI-AML3 = 3 μM; KG-1 = 3 μM; MV4-11 = 3 μM; MOLM-13 = 3 μM; KASUMI-1 = 3 μM) for 24 h. β-actin was used for loading normalization. In the lower part of the figure histograms represent the average signal obtained from relative band quantification of at least three independent experiments. **H** Histograms showing the percentage of pH2AX$^+$/pMPM2$^+$ cells in AML cell lines treated with GO (KASUMI-1 = 1.97 ng/mL, MOLM-13 = 1.97 ng/mL, OCI-AML3 = 1473 ng/mL, MV4-11 = 1473 ng/mL and KG-1 = 1473 ng/mL) for 48 h and with talazoparib (IC_{50} values after 24 h of treatment) for additional 6 h. **I** Comet assay in OCI-AML3 cell line treated with γ-calicheamicin (IC_{50} value) in combination with talazoparib (IC_{50} value) for 18 h. In the lower part of the figure scatter-plots with histograms show the variation of Tail Area, Tail Length and Tail moment between controls and treatments. **J** Clonogenic results of MV4-11, KG-1, OCI-AML3, MOLM-13 and KASUMI-1 cells treated with sub-toxic concentrations of γ-calicheamicin (OCI-AML3: 5 pM; KG-1: 7.5 pM; MV4-11: 2 pM; MOLM-13: 0.3 pM; KASUMI-1:0.02 pM) and talazoparib (OCI-AML3: 0.166 μM; KG-1: 0.05 μM; MV4-11: 0.33 μM; MOLM-13: 0.06 μM; KASUMI-1:0.11 μM) for 10–14 days. **K** Clonogenic results of MV4-11, KG-1, OCI-AML3, MOLM-13 and KASUMI-1 cells treated with sub-toxic concentrations of GO (OCI-AML3 = 1473 ng/mL; KG-1 = 1473 ng/mL; MV4-11 = 1473 ng/mL; MOLM-13 = 1.97 ng/mL; KASUMI-1 = 1.97 ng/mL) and talazoparib (OCI-AML3: 0.166 μM; KG-1: 0.05 μM; MV4-11: 0.33 μM; MOLM-13: 0.06 μM; KASUMI-1:0.11 μM) for 10–14 days

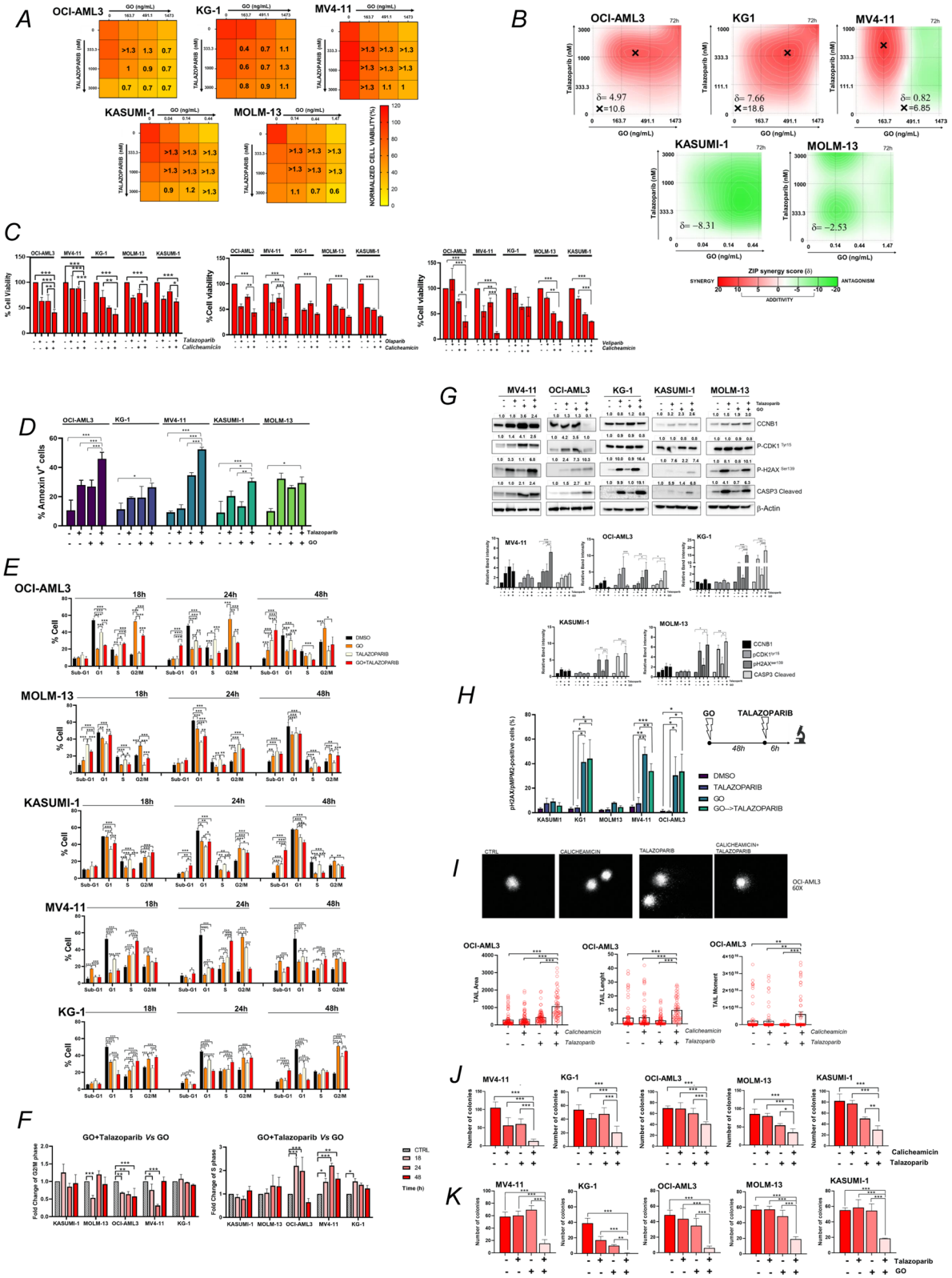

Fig. 4 (See legend on previous page.)

also for AML cell lines the effect of the combination on clonogenic capacity. We found that in all the treated AML cell lines, the prolonged treatment with talazoparib and calicheamicin significantly reduced the clonogenic capacity compared to control and single treatments. Interestingly, also MOLM-13 and KASUMI-1 cells which showed antagonistic response in the combination index analysis were significantly sensitive to the combination in terms of reduction of clonogenic capacity. These data suggested that in AML cell lines the effect of the combination is delayed compared to ALL cells (Fig. 4J). Similar results were observed when evaluating the effect of GO and talazoparib on the reduction of clonogenic capacity in AML cell lines. (Fig. 4K)

The inhibition of PARPs functionality synergized with INO against ALL primary leukemic cells and partially with GO against AML primary leukemic cells

The efficacy of the two combinations was then evaluated in primary ALL (n = 5) and AML (n = 5) samples (Table S6 for patients' characteristics). The combination of INO and talazoparib reduced cell viability in all ALL samples in a dose- and time-dependent manner to varying degrees (Fig. 5A; S5A). Interestingly, the efficacy of the combination in terms of Z scores increased over time in the majority of samples (Fig. 5A; S5B). Primary AML samples responded heterogeneously to the combination of GO and talazoparib shifting from synergism (AML#3) to antagonism (AML#1, Fig. 5B). In contrast to ALL primary cells, in AML the strongest effect was observed 24 h after exposure, with strong synergism in AML#2, AML#3 and AML#4, compared to later time points (Fig.S6A-B).

Discussion

Our study investigated whether the effectiveness of ADCs is associated with acute leukemia cells' ability to repair calicheamicin-induced DNA damage. Preclinical data supports this proposal, indicating the efficacy of combining ADCs with selective DDR inhibitors [45–48]. Here, we evaluated whether the inhibition of PARPs functionality, using talazoparib, could enhance the cytotoxicity of GO and INO against AML and ALL cells, respectively. We found that, at least in vitro, the response to INO does not strictly correlate with the expression of CD22 on ALL cell lines. The available in vivo data on the correlation between CD22 expression INO efficacy suggest that low CD22 expression is a marker of good response to INO-based therapies [49]. Conversely, ALL patients expressing the highest level of CD22 seem to benefit more of INO-based treatments [50]. Instead in AML cells, in line with clinical observations [39, 40], we found a correlation between CD33 expression and the in vitro response to GO. However, our data showed a concordance between response to ADCs and γ-calicheamicin (the cytotoxic payload of GO and INO) in AML and ALL cell lines, suggesting a driver role of cell sensitivity to γ-calicheamicin over target expression.

To deeper understand the response to γ-calicheamicin-induced DNA damages and to confirmed the rationale for combining ADCs with PARP1 inhibitors, we studied cell cycle and pathway alterations. We observed that INO and GO caused a robust G2/M cell-cycle arrest in acute leukemia cell lines, as confirmed by increased levels of pCDK1^{Tyr15} (MPF complex inactive [51]) in ALL. In AML cell lines only OCI-AML3 and KG-1 showed a significant inactivation of the MPF complex following treatment.

In ALL cells INO strongly induced the DNA damage as showed by enhanced pH2AX^{Ser139} after treatment. Similar results were observed in KASUMI-1, MOLM-13 and OCI-AML3 cells, while only a weak increase of pH2AX^{Ser139} was seen in MV4-11 and KG-1 cells. Looking specifically to the G2/M cell cycle checkpoint activation following γ-calicheamicin-induced DNA damage, we found that ALL cell lines responded to calicheamicin activating the ATM/CHK1/CHK2 pathway. Regarding AML models, only MV4-11 and KG-1 cells activated the same pathway.

Among different PARP1 inhibitors (veliparib, olaparib, and talazoparib), talazoparib exhibited the most pronounced cytotoxic effects across all cell lines, and particularly in ALL ones. Overall, our data suggests that ALL cell lines are more sensitive to PARP1 inhibitors compared to AML cells and this difference is not related to the presence of genomic alterations in DNA damage repair genes. Conversely, ALL cell lines exhibited elevated expression levels of key DNA repair proteins

(See figure on next page.)

Fig. 5 Reduction of cell viability of primary leukemic ALL and AML cells treated with talazoparib in combination with INO and GO, respectively. **A** Cell viability analysis and Zero Interaction Potency (ZIP) score of bone marrow or peripheral blood cells from adult ALL patients (n = 5) treated with escalating concentrations of talazoparib and INO for 72 h. In the histograms, viable cells are shown as a percentage of the control cell (DMSO-treated), while the two-dimensional synergy map shows the ZIP score for each drug combination. **B** Cell viability analysis and ZIP scores of bone marrow or peripheral blood cells from adult AML patients (n = 5) treated with escalating concentrations of talazoparib and GO for 72 h. In the histograms, viable cells are shown as a percentage of the control cell (DMSO-treated), while the two-dimensional synergy map shows the ZIP score for each drug combination. The patient-specific drug concentrations are reported in the figure axes

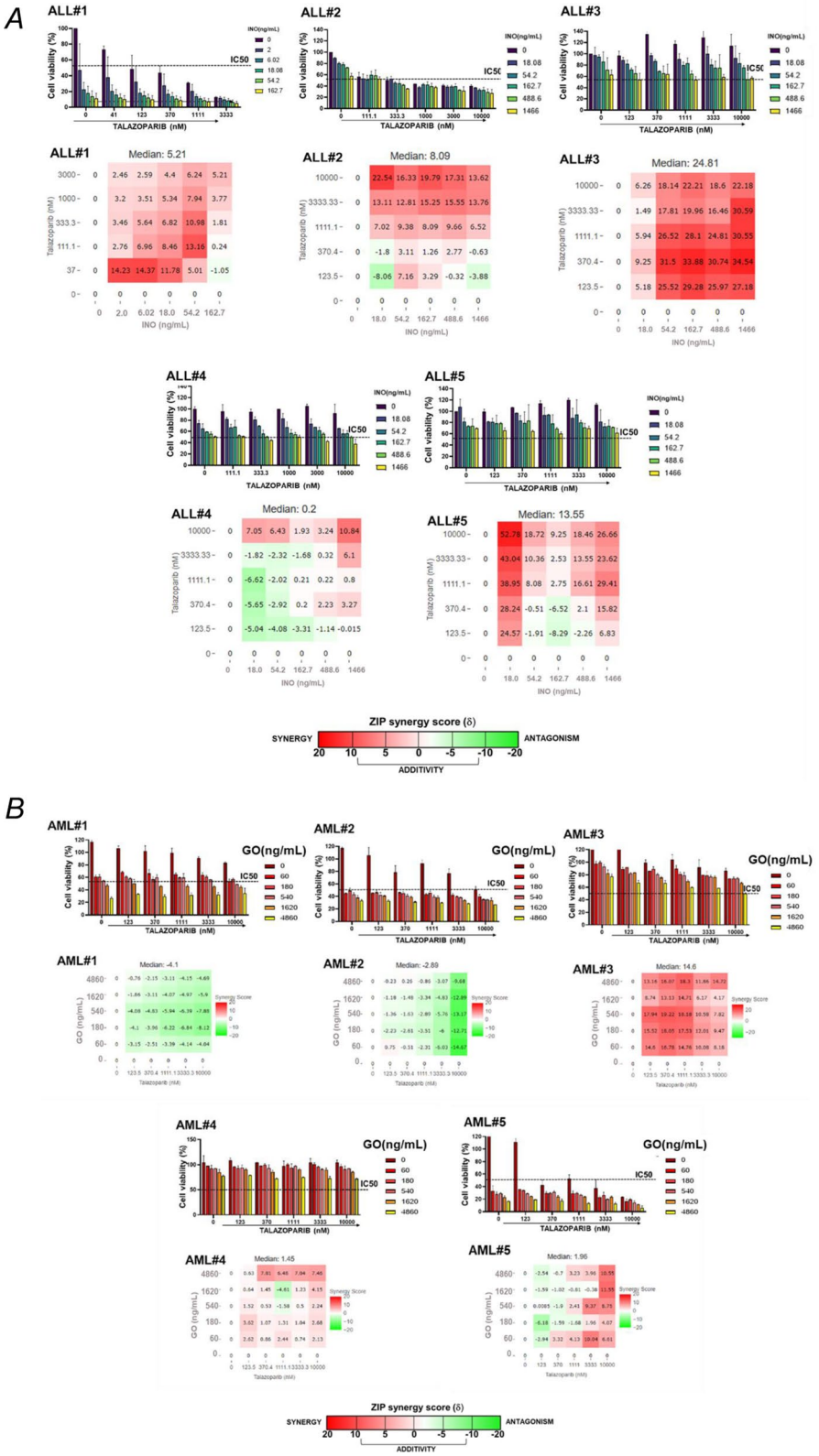

Fig. 5 (See legend on previous page.)

compared to AML cell lines. In line with the observed response to PARPs inhibition in monotherapy, ALL cell lines were more sensitive to UV-damages compared with AML cells. UV-ray was chosen as a non-chemical source of DNA damages in order to evaluate the intrinsic DDR-proficiency of our panel of acute leukemia cell lines, since the response is mediated by PARP1 [52, 53].

We then evaluated the effect of combining talazoparib with INO or GO on ALL and AML cell lines, respectively. We here report, for the first time based on our knowledge, the synergistic effect of INO and talazoparib combination in ALL cell lines and primary ALL leukemic cells, as supported by combination index analysis, Z-synergy score, induction of cell death and DNA damage and clonogenic analysis. Interestingly, cell-cycle analyses suggested that the efficacy of the combination may be related to the ability of talazoparib to abrogate the G2/M cell-cycle checkpoint induced by INO. In this scenario, the cell lines with the lowest G2/M phase fold-changes (INO versus INO + talazoparib) showed the strongest effect in terms of reduction of cell viability, induction of apoptosis and inhibition of clonogenic capacity. From a biological point of view, our Comet assay data, suggest that PARP1 is directly involved in the response and repair of γ-calicheamicin induced DNA damages. Regarding AML cell lines, some preclinical in vitro and in vivo preliminary data regarding the efficacy of talazoparib in combination with GO have been previously reported [46]. Here we evaluated the efficacy of the combination in AML cell lines with diverse molecular backgrounds and in a small panel of primary AML cells. The response to the combination was heterogenous both in AML cell lines and primary leukemic cells. We observed a synergistic effect of the combination in OCI-AML3, KG-1 and MV4-11 AML models, while we found poor additive or antagonistic effect in MOLM-13 and KASUMI-1 cells. Again, cell-cycle profile data suggested that the highest sensitivity to the combination (OCI-AML3 and MV4-11) was coupled with the lowest G2/M fold-change (GO versus GO + talazoparib). Although, combination index and apoptosis analyses reported heterogenous response to the combination, clonogenic assay showed that the long-term treatment with talazoparib and γ-calicheamicin significantly reduced the number of colonies in all the AML cell lines compared to controls and single treatments. These data suggest that AML may have a delayed response to the combination compared to ALL cells. This hypothesis may be supported by the absence of increased pH2AX + /pMPM2 + cells in the samples treated with the combination compared to GO alone (6 h of co-treatment) and instead by the increased of overall genotoxicity (Comet assay and immunoblotting analysis) seen after 18 h of co-treatments. In ALL cells everything seems earlier as cells showed increased DNA damages in the combinations even after 6 h of co-treatment.

Evaluation of primary AML and ALL samples further demonstrated varying responses to the combination treatments, with ALL cells consistently showing increased sensitivity to the INO and talazoparib combination compared to AML cells. However, responses varied among individual patient samples, suggesting the importance of patient-specific factors in treatment outcomes that need to be further investigated in larger patient cohorts.

Conclusion

Our findings underscore the potential of combining PARP1 inhibition with ADCs to enhance therapeutic efficacy in acute leukemias, particularly in ALL. Our results provide data on the direct involvement of PARPs protein in the response and repair of γ-calicheamicin-induced DNA damages. Talazoparib demonstrated promising cytotoxic effects and synergistic interactions with INO, highlighting its potential as a therapeutic adjunct in the treatment of acute leukemias. Clinical validation of these findings is warranted to exploit the therapeutic potential of these combinations in clinical settings.

Supplementary Information

The online version contains supplementary material available at https://doi.org/10.1186/s12967-024-05838-9.

Supplementary Material 1.
Supplementary Material 2.
Supplementary Material 3.
Supplementary Material 4.
Supplementary Material 5.
Supplementary Material 6.
Supplementary Material 7.
Supplementary Material 8.

Acknowledgements
This study was founded by Pfizer Oncology (ref. WI246501, for efficacy tests), AIRC IG 2019 within the Project Code: 23810 (PI Martinelli G., for functional analyses).

Author contributions
AGLDR designed experiments, analyzed data, and wrote the manuscript; MJ, AP, AM, CM, MG, FO, LL, AF, MTB, MP, ZM, CA, and SC provided technical assistance, performed experiments and analyzed data. AF, GiM, SG, MR, MG, ME, DO and AE contributed to patient management and primary leukemic sample collection. GS cooperate in the writing, reviewed the data, and GM coordinated the research. All authors read and approved the final manuscript.

Data availability
Not applicable.

Declarations

Competing interests

GM has competing interests with Novartis, BMS, Roche, Pfizer, ARIAD, MSD.

Author details

[1]Biosciences Laboratory, IRCCS Istituto Romagnolo per lo Studio dei Tumori (IRST) "Dino Amadori", Via Piero Maroncelli, 40, 47014 Meldola, FC, Italy. [2]Fondazione Pisana per la Scienza ONLUS, San Giuliano Terme, Italy. [3]Present Address: Wellmicro SPA, Bologna, Italy. [4]Pharmacy, IRCCS Istituto Romagnolo per lo Studio dei Tumori (IRST) "Dino Amadori", Via Piero Maroncelli, 40, 47014 Meldola, FC, Italy. [5]Department of Clinical and Experimental Medicine, Section of Hematology, University of Pisa, 56126 Pisa, Italy. [6]Onco Hematology, Department of Oncology, Veneto Institute of Oncology, Istituto Oncologico Veneto-Istituto di Ricerca e Cura a Carattere Scientifico (IOV-IRCCS), Castelfranco Veneto, Italy. [7]Hematology Unit & Romagna Transplant Network, Ravenna Hospital, Ravenna, Italy. [8]Azienda ULSS 2 Marca Trevigiana Ospedale Ca' Foncello, Treviso, Italy. [9]UOC di Ematologia, Dipartimento di Oncologia Ematologia, Ospedale Santo Spirito, Pescara, Italy. [10]Hematology Unit, Presidio Ospedaliero Molinette, A.O.U. Città della Salute e Della Scienza, Turin, Italy. [11]IRCCS Istituto Romagnolo per lo Studio dei Tumori (IRST) "Dino Amadori", Via Piero Maroncelli, 40, 47014 Meldola, FC, Italy.

Received: 9 July 2024 Accepted: 31 October 2024
Published online: 26 November 2024

References

1. Walter RB. Brief overview of antibody–drug conjugate therapy for acute leukemia. Expert Opin Biol Ther. 2021. https://doi.org/10.1080/14712598.2020.1817373.
2. Kantarjian HM, DeAngelo DJ, Stelljes M, Liedtke M, Stock W, Gökbuget N, et al. Inotuzumab ozogamicin versus standard of care in relapsed or refractory acute lymphoblastic leukemia: final report and long-term survival follow-up from the randomized, phase 3 INO-VATE study. Cancer. 2019. https://doi.org/10.1002/cncr.32116.
3. Jabbour E, Paul S, Kantarjian H. The clinical development of antibody–drug conjugates—lessons from leukaemia. Nat Rev Clin Oncol. 2021;18:418–33.
4. Gottardi M, Sperotto A, Di Rorà AGL, Padella A, Cangini D, Giannini MB, et al. Gemtuzumab ozogamicin in acute myeloid leukemia: PAST, present and future. Minerva Med. 2020;111:395–410.
5. Khongorzul P, Ling CJ, Khan FU, Ihsan AU, Zhang J. Antibody-drug conjugates: a comprehensive review. Mol Cancer Res. 2020;18:3–19.
6. Lamarr WA, Yu L, Nicolaou KC, Dedon PC. Supercoiling affects the accessibility of glutathione to DNA-bound molecules: positive supercoiling inhibits calicheamicin-induced DNA damage. Proc Natl Acad Sci USA. 1998. https://doi.org/10.1073/pnas.95.1.102.
7. Elmroth K, Nygren J, Mårtensson S, Ismail IH, Hammarsten O. Cleavage of cellular DNA by calicheamicin γ1. DNA Repair. 2003;2:363–74.
8. Dedon PC, Salzberg AA, Xu J. Exclusive production of bistranded DNA damage by calicheamicin. Biochemistry. 1993. https://doi.org/10.1021/bi00065a013.
9. Lambert J, Pautas C, Terré C, Raffoux E, Turlure P, Caillot D, et al. Gemtuzumab ozogamicin for de novo acute myeloid leukemia: final efficacy and safety updates from the open-label, phase III ALFA-0701 trial. Haematologica. 2019;104:113–9.
10. Gottardi M, Simonetti G, Sperotto A, Nappi D, Di Ghelli Luserna Rorà A, Padella A, et al. Therapeutic targeting of acute myeloid leukemia by gemtuzumab ozogamicin. Cancers. 2021;13:4566.
11. Kantarjian HM, DeAngelo DJ, Stelljes M, Martinelli G, Liedtke M, Stock W, et al. Inotuzumab ozogamicin versus standard therapy for acute lymphoblastic leukemia. N Engl J Med. 2016. https://doi.org/10.1056/NEJMoa1509277.
12. DiJoseph JF, Armellino DC, Boghaert ER, Khandke K, Dougher MM, Sridharan L, et al. Antibody-targeted chemotherapy with CMC-544: a CD22-targeted immunoconjugate of calicheamicin for the treatment of B-lymphoid malignancies. Blood. 2004;103:1807–14.
13. Kantarjian HM, Boissel N, Papayannidis C, Luskin MR, Stelljes M, Advani AS, et al. Inotuzumab ozogamicin in adult acute lymphoblastic leukemia: development, current status, and future directions. Cancer. 2024. https://doi.org/10.1002/cncr.35505.
14. Marks DI, Kebriaei P, Stelljes M, Gökbuget N, Kantarjian H, Advani AS, et al. Outcomes of allogeneic stem cell transplantation after inotuzumab ozogamicin treatment for relapsed or refractory acute lymphoblastic leukemia. Biol Blood Marrow Transpl. 2019;25:1720–9.
15. Collins DM, Bossenmaier B, Kollmorgen G, Niederfellner G. Acquired resistance to antibody-drug conjugates. Cancers. 2019;11:394.
16. Fenwarth L, Fournier E, Cheok M, Boyer T, Gonzales F, Castaigne S, et al. Biomarkers of gemtuzumab ozogamicin response for acute myeloid leukemia treatment. Int J Mol Sci. 2020. https://doi.org/10.3390/ijms21165626.
17. Balaian L, Ball ED. Cytotoxic activity of gemtuzumab ozogamicin (Mylotarg) in acute myeloid leukemia correlates with the expression of protein kinase Syk. Leukemia. 2006. https://doi.org/10.1038/sj.leu.2404437.
18. Rafiee R, Chauhan L, Alonzo TA, Wang YC, Elmasry A, Loken MR, et al. ABCB1 SNP predicts outcome in patients with acute myeloid leukemia treated with Gemtuzumab ozogamicin: a report from Children's Oncology Group AAML0531 Trial. Blood Cancer J. 2019. https://doi.org/10.1038/s41408-019-0211-y.
19. Short NJ, Richard-Carpentier G, Kanagal-Shamanna R, Patel KP, Konopleva M, Papageorgiou I, et al. Impact of CD33 and ABCB1 single nucleotide polymorphisms in patients with acute myeloid leukemia and advanced myeloid malignancies treated with decitabine plus gemtuzumab ozogamicin. Am J Hematol. 2020. https://doi.org/10.1002/ajh.25854.
20. Diaz-Flores E, Wintering A, Ishiyama K, Tamaki S, Tamaki C, Fandel J, et al. CD22 low/Bcl-2 high expression identifies poor response to inotuzumab in relapsed/ refractory acute lymphoblastic leukemia. Blood. 2021. https://doi.org/10.1182/blood-2021-149037.
21. Lanza F, Maffini E, Rondoni M, Massari E, Faini AC, Malavasi F. CD22 expression in b-cell acute lymphoblastic leukemia: biological significance and implications for inotuzumab therapy in adults. Cancers. 2020. https://doi.org/10.3390/cancers12020303.
22. Takeshita A, Shinjo K, Yamakage N, Ono T, Hirano I, Matsui H, et al. CMC-544 (inotuzumab ozogamicin) shows less effect on multidrug resistant cells: analyses in cell lines and cells from patients with B-cell chronic lymphocytic leukaemia and lymphoma. Br J Haematol. 2009. https://doi.org/10.1111/j.1365-2141.2009.07701.x.
23. Lord CJ, Ashworth A. The DNA damage response and cancer therapy. Nature. 2012;481:287–94.
24. Padella A, Di Ghelli Luserna Rorà A, Marconi G, Ghetti M, Martinelli G, Simonetti G. Targeting PARP proteins in acute leukemia: DNA damage response inhibition and therapeutic strategies. J Hematol Oncol. 2022. https://doi.org/10.1186/s13045-022-01228-0.
25. Padella A, Fontana MC, Marconi G, Fonzi E, Petracci E, Ferrari A, et al. Loss of PALB2 predicts poor prognosis in acute myeloid leukemia and suggests novel therapeutic strategies targeting the DNA repair pathway. Blood Cancer J. 2021. https://doi.org/10.1038/s41408-020-00396-x.
26. Caldecott KW. Single-strand break repair and genetic disease. Nat Rev Genet. 2008;9:619–31.
27. Helleday T, Bryant HE, Schultz N. Cell cycle poly(ADP-ribose) polymerase (PARP-1) in homologous recombination and as a target for cancer therapy. Cell Cycle. 2005;4:9.
28. Han Y, Jin F, Xie Y, Liu Y, Hu S, Liu XD, et al. DNA-PKcs PARylation regulates DNA-PK kinase activity in the DNA damage response. Mol Med Rep. 2019;20:3609.
29. Kontandreopoulou C-N, Diamantopoulos PT, Tiblalexi D, Giannakopoulou N, Viniou N-A. PARP1 as a therapeutic target in acute myeloid leukemia and myelodysplastic syndrome. Blood Adv. 2021. https://doi.org/10.1182/bloodadvances.2021004638.
30. Li X, Li C, Jin J, Wang J, Huang J, Ma Z, et al. High PARP-1 expression predicts poor survival in acute myeloid leukemia and PARP-1 inhibitor and SAHA-bendamustine hybrid inhibitor combination treatment synergistically enhances anti-tumor effects. EBioMedicine. 2018;38:47–56.
31. Giorgi M, Portwood SM, Boncek M, Wang ES. PARP inhibition with talazoparib enhances DNA damage and anti-leukemic activity of venetoclax in preclinical human acute myeloid leukemia (AML) models. Blood. 2021;138:1176–1176.

32. Molenaar RJ, Radivoyevitch T, Nagata Y, Khurshed M, Przychodzen B, Makishima H, et al. Idh1/2 mutations sensitize acute myeloid leukemia to parp inhibition and this is reversed by idh1/2-mutant inhibitors. Clin Cancer Res. 2018;24:1705–15.
33. Iacobucci I, Qu C, Varotto E, Janke LJ, Yang X, Seth A, et al. Modeling and targeting of erythroleukemia by hematopoietic genome editing. Blood. 2021;137:1628–40.
34. Tothova Z, Valton A-L, Gorelov R, Vallurupalli M, Krill-Burger JM, Holmes A, et al. Cohesin mutations alter DNA damage repair and chromatin structure and create therapeutic vulnerabilities in MDS/AML. JCI Insight. 2020. https://doi.org/10.1172/jci.insight.142149.
35. Baer MR, Kogan AA, Bentzen SM, Mi T, Lapidus RG, Duong VH, et al. Phase I clinical trial of DNA methyltransferase inhibitor decitabineand PARP inhibitor talazoparib combination therapy in relapsed/refractory acute-myeloid leukemia. Clin Cancer Res. 2022;28:1313.
36. Yadav B, Wennerberg K, Aittokallio T, Tang J. Searching for drug synergy in complex dose-response landscapes using an interaction potency model. Comput Struct Biotechnol J. 2015;13:504–13.
37. Hanasoge S, Ljungman M. H2AX phosphorylation after UV irradiation is triggered by DNA repair intermediates and is mediated by the ATR kinase. Carcinogenesis. 2007. https://doi.org/10.1093/carcin/bgm157.
38. Di Rorà AGL, Bocconcelli M, Ferrari A, Terragna C, Bruno S, Imbrogno E, et al. Synergism through WEE1 and CHK1 inhibition in acute lymphoblastic leukemia. Cancers. 2019;11:1654.
39. Walter RB, Gooley TA, Van Der Velden VHJ, Loken MR, Van Dongen JJM, Flowers DA, et al. CD33 expression and P-glycoprotein–mediated drug efflux inversely correlate and predict clinical outcome in patients with acute myeloid leukemia treated with gemtuzumab ozogamicin monotherapy. Blood. 2007;109:4168–70. https://doi.org/10.1182/blood-2006-09-047399.
40. Pollard JA, Loken M, Gerbing RB, Raimondi SC, Hirsch BA, Aplenc R, et al. CD33 expression and its association with gemtuzumab ozogamicin response: results from the randomized phase III children's oncology group trial AAML0531. J Clin Oncol. 2016;34:747–55.
41. Murai J, Huang SYN, Renaud A, Zhang Y, Ji J, Takeda S, et al. Stereospecific PARP trapping by BMN 673 and comparison with olaparib and rucaparib. Mol Cancer Ther. 2014;13:433.
42. Sondka Z, Dhir NB, Carvalho-Silva D, Jupe S, McLaren K, Starkey M, et al. COSMIC: a curated database of somatic variants and clinical data for cancer. Nucl Acids Res. 2024;52:1210–7. https://doi.org/10.1093/nar/gkad986.
43. Barretina J, Caponigro G, Stransky N, Venkatesan K, Margolin AA, Kim S, et al. The cancer cell line encyclopedia enables predictive modeling of anticancer drug sensitivity. Nature. 2012;483:603.
44. Escargueil AE, Larsen AK. Mitosis-specific MPM-2 phosphorylation of DNA topoisomerase IIα is regulated directly by protein phosphatase 2A. Biochem J. 2007;403:235.
45. Yamauchi T, Uzui K, Nishi R, Shigemi H, Ueda T. Gemtuzumab ozogamicin and olaparib exert synergistic cytotoxicity in CD33-positive HL-60 myeloid leukemia cells. Anticancer Res. 2014;34:5487–94.
46. Portwood SM, Cantella MC, Cronin TL, Wang ES. Addition of the PARP inhibitor, talazoparib, to gemtuzumab ozogamicin significantly enhances anti-leukemic activity in human CD33+ acute myeloid leukemia. Blood. 2019;134:1371–1371.
47. Tirrò E, Massimino M, Romano C, Pennisi MS, Stella S, Vitale SR, et al. Chk1 inhibition restores inotuzumab ozogamicin citotoxicity in CD22-positive cells expressing mutant p53. Front Oncol. 2019. https://doi.org/10.3389/fonc.2019.00057.
48. Carr MI, Zimmermann A, Chiu LY, Zenke FT, Blaukat A, Vassilev LT. DNA-PK inhibitor, M3814, as a new combination partner of mylotarg in the treatment of acute myeloid leukemia. Front Oncol. 2020;10:127.
49. Shah NN, O'Brien MM, Yuan C, Ji L, Xu X, Rheingold SR, et al. Evaluation of CD22 modulation as a mechanism of resistance to inotuzumab ozogamicin (InO): results from central CD22 testing on the Children's Oncology Group (COG) phase II trial of INO in children and young adults with CD22+ B-acute lymphoblastic leukemi. J Clin Oncol. 2020. https://doi.org/10.1200/JCO.2020.38.15_suppl.10519.
50. Kantarjian HM, Stock W, Cassaday RD, DeAngelo DJ, Jabbour E, O'Brien SM, et al. Inotuzumab ozogamicin for relapsed/refractory acute lymphoblastic leukemia in the INO-VATE trial: CD22 pharmacodynamics, efficacy, and safety by baseline CD22. Clin Cancer Res. 2021. https://doi.org/10.1158/1078-0432.CCR-20-2399.
51. Di Ghelli Luserna Rorà A, Martinelli G, Simonetti G. The balance between mitotic death and mitotic slippage in acute leukemia: a new therapeutic window? J Hematol Oncol. 2019;12:1–16.
52. Purohit NK, Robu M, Shah RG, Geacintov NE, Shah GM. Characterization of the interactions of PARP-1 with UV-damaged DNA in vivo and in vitro. Sci Rep. 2016;6:1–11.
53. Robu M, Shah RG, Petitclerc N, Brind'amour J, Kandan-Kulangara F, Shah GM. Role of poly(ADP-ribose) polymerase-1 in the removal of UV-induced DNA lesions by nucleotide excision repair. Proc Natl Acad Sci USA. 2013;110:1658–63.

Publisher's Note